Article ID: 1006-8775(2023) 02-0252-12

Study on the Formation Mechanism and Microphysical Characteristics of Warm-Sector Convective System with Multiple-Rain-Bands Organizational Mode

ZHANG Hong-hao (张弘豪)[1, 2], GUO Ze-yong (郭泽勇)[1, 2], LI Hui-qi (黎慧琦)[3, 4], HU Zhi-qun (胡志群)[1], CHEN Xing-deng (陈星登)[1, 2], LIN Qing (林 青)[5], XIA Feng (夏 丰)[3]

(1. State Key Laboratory of Severe Weather, Chinese Academy of Meteorological Sciences, Beijing 100081 China;
2. Yangjiang Meteorological Bureau, China Meteorological Administration, Yangjiang, Guangdong 529500 China;
3. Institute of Tropical and Marine Meteorology, China Meteorological Administration, Guangzhou 510641 China;
4. China Meteorological Administration Tornado Key Laboratory, Guangzhou 510641 China;
5. Guangdong Meteorological Observatory, Guangzhou 510641 China)

Abstract: Based on ERA5 reanalysis data and multi-source observations, including polarimetric radar and automatic weather stations, this study analyzes the formation mechanism and microphysical characteristics of a warm-sector heavy rainfall event caused by a convective system with multiple-rain-bands organizational mode over the western coast of south China. In the early stage, under the influence of coastal convergence and topography, convection was triggered in the coastal mountainous areas and moved north-eastwards. Nocturnal cooling induced the north winds in the inland mountainous area. A mesoscale convergence line was formed in the middle of Yangjiang city between the inland north and coastal south winds, which facilitated the developing and merging of convective storms into a linear convective band along the convergence line. This relatively long convective band presented a quasi-stationary state in the south of Mt. Ehuangzhang and Mt. Tianlu, which results in the first precipitation peak. At this stage, the convection developed to a higher level, with relatively larger raindrops, producing larger amounts of rainfall, which was probably related to the active merging of convection. In the later phase, as the environmental winds shifted, convective bands tended to move southeastwards, accompanied with the cold pools. At the same time, the multiple short convective bands were formed, which were almost parallel to the shear line, and a multiple-rain-bands organizational mode occurred. The mesoscale convergence line maintained due to the outflows of cold pools caused by precipitation in the preceding period, and then gradually moved southwards. Under the influence of the mesoscale convergence and topography, convection was continuously triggered at the southern end of the short convective bands. This back-building characteristic favored the development of the convective system. The multiple rain bands passed through the same place in a "rainband-training" form, resulting in the second peak of precipitation. The collision process was active in the low levels during this event.

Key words: multiple-rain-bands; warm sector heavy rainfall; south China

CLC number: P458.1+21 **Document code:** A

Citation: ZHANG Hong-hao, GUO Ze-yong, LI Hui-qi, et al. Study on the Formation Mechanism and Microphysical Characteristics of Warm-Sector Convective System with Multiple-Rain-Bands Organizational Mode [J]. Journal of Tropical Meteorology, 2023, 29(2): 252-263, https://doi.org/10.46267/j.1006-8775.2023.018

1 INTRODUCTION

Warm-sector heavy rainfall characterized by mesoscale convection often hits south China, leading to severe disasters. The intensity of warm-sector rainfall is even greater than that of the frontal rainfall (Lin et al.[1]; Li[2]). In recent years, high-resolution numerical models have significantly improved the forecasting accuracy of heavy rainfall in south China, but it is still difficult to forecast warm-sector heavy rainfall. Insufficient understanding of the formation mechanism of warm-sector heavy rainfall has hindered further improvement of the numerical model for forecasting heavy rainfall.

Many researchers have studied the environmental conditions and the thermodynamics characteristics of the warm-sector heavy rainfall over south China (Wu and Luo[3]; Qian et al.[4]; Miao et al.[5]; Du and Chen[6]; Huang et al.[7−8]; Liang et al.[9]; Wu et al.[10]; Liang and Gao[11]; Du et al.[12]). According to a statistical study by Wu et al.[13], warm-sector heavy rainfall frequently occurs in the coastal area of Guangdong, which peaks in the early morning because of the enhanced convergence between land breezes and nocturnal low-level jets. Du and Chen[6] proposed a conceptual model of warm-sector

Received 2022-09-14; **Revised** 2023-02-15; **Accepted** 2023-05-15

Funding: The Open Grants of the State Key Laboratory of Severe Weather (2020LASW-B04); National Natural Science Foundation of China (U2242203, 41905047); Guangdong Province Important Area Research and Development Plan (2020B1111200001); Operation-oriented Research Project of Guangdong Meteorological Bureau (GRMC2022M31); The Joint Research Project for Meteorological Capacity Improvement (22NLTSQ003); Guangdong Basic and Applied Basic Research Foundation (2023A1515011971)

Biography: ZHANG Hong-hao, Engineer, primarily undertaking research on weather forecasting.

Corresponding author: LI Hui-qi, e-mail: lihq@gd121.cn

heavy rainfall, which is triggered by the combination of double low-level jets. Wang et al.[14] found that the change of low-level synoptic situation played a key role in determining the distribution of heavy rainfall in the coastal areas of south China. Some scholars discussed different roles of topography, urban environment, land-sea contrast in the convective initiation and development during warm-sector heavy rainfall events (Huang et al.[7]; Du et al.[15]; Yin et al.[16]; Li et al. [17]; Gao et al.[18]; Zhang et al.[19]).

Warm-sector heavy rainfall events are mainly caused by mesoscale convective systems (MCSs) (He et al.[20]). Based on radar observations, researchers have studied the organizational modes of MCSs associated with warm-sector heavy rainfall. For example, Wang et al.[21] found the characteristics of rainband training and echo training in a warm sector heavy rainfall event along the western coast of Guangdong. Li et al.[22] used 14-year radar observations to classify the MCSs associated with warm-sector heavy rainfall over south China into nine organizational modes, including a nonlinear mode and eight linear modes. Among these organizational modes, Multiple-Rain-Band (MRB) mode is a special type which is rarely investigated in other regions (Parker and Johnson[23]; Schumacher and Johnson[24]; Gallus Jr et al.[25]; Zheng et al.[26]). So far, there are only a few studies on the formation mechanism of MRB-type MCSs. Wang et al.[21] pointed out that the topography, near-surface winds, upstream warm advections, and the cold pool outflows were important in triggering and maintaining the MCSs characterized by echo training and rainband training. Liu et al.[27] analyzed the influence of mesoscale outflow boundary and the rapid splitting and reestablishment process on the formation of MCSs comprised of MRB over coastal south China.

On the other hand, with the increasing deployment of dual-polarization radar and two-dimensional video disdrometers over south China (Zhao et al.[28]; Liu et al.[29]), the convective properties or microphysical characteristics of warm-sector heavy rainfall have been studied in recent years (e. g., Li et al.[30]; Han et al.[31]; Wang et al.[32]). Li et al.[30] shows that the storm producing extreme rainfall over Guangzhou on 7 May 2017 has active warm-rain microphysical processes and a large number of moderate-to-large raindrops. Han et al.[31] compared the microphysical characteristics of the coexisting warm-sector rainfall and frontal rainfall. More intense convection, larger raindrops, and higher liquid water content were found in the warm-sector heavy rainfall. However, the microphysical characteristics of MRB-type MCSs are rarely studied. Therefore, it is necessary to further study the formation mechanism as well as the microphysical characteristics of the MRB-type MCSs, so as to further gain insights into the formation of the warm-sector heavy rainfall over south China.

Yangjiang, located on the western coast of south China, is one of the heaviest precipitation centers in south China (Luo et al.[33]). This paper is intended to study the formation mechanism and microphysical properties of the MRB-type convective system producing heavy rainfall under the warm-sector situation in Yangjiang on June 2, 2020. The formation process of the MRB organization mode in this case is somewhat different from that of previous studies (e. g., Wang et al.[21]; Liu et al.[27]), which is worth of in-depth investigation. A linear convective band was formed in the earlier period and the convective system later transformed into the MRB mode.

The remainder of this work is organized as follows. Section 2 describes the data and methods. Section 3 provides an overview of this event, including the evolution of convective systems. Section 4 discusses how the MRB organizational mode was formed. The microphysical characteristics of the convective system are analyzed in section 5. The final section gives a summary and conclusions.

2 DATA AND METHODS

2.1 *Data*

In this study, ERA5 reanalysis data at a horizontal spatial resolution of 0.25 ° × 0. 25 ° and a time resolution of one hour, and the sounding data at Yangjiang (station number: 59663) were used to analyze the synoptic background. Surface observations in Guangdong province, and Yangjiang, Guangzhou, Zhaoqing, and Zhanjiang S-band dual-polarization radar observations (marked as YJ-SPOL, GZ-SPOL, ZQ-SPOL and ZJ-SPOL, respectively in Fig. 1) were used to perform mesoscale and convective-scale analysis.

2.2 *Processing of radar data*

Firstly, the polarimetric radar data were quality controlled using the micro-raindrop method and linear programming method. Then, the radar data were bilinearly interpolated to three-dimensional Cartesian coordinates with a horizontal resolution of 1 km and a vertical resolution of 0.5 km. The weighted average method was used to combine the gridded observations of the four radars (Zhang et al.[34]).

The constrained-gamma model developed by Zhang et al.[35] and the localized empirical relationship obtained by Liu et al.[36] were used to retrieve the raindrop size distributions from the polarimetric variables. The mass-weighted mean diameter (D_m, mm), and the normalized intercept parameter (N_w, m^{-3} mm^{-1}) can be further derived based on the gamma raindrop size distribution.

3 CASE OVERVIEW

3.1 *Overview of the rainfall*

On June 2, 2020, heavy rainfall occurred on the west coast (between Maoming and Jiangmen) of Guangdong (Fig. 2a). The heavy rainfall flooded many roads, houses, farmlands, etc., causing economic losses

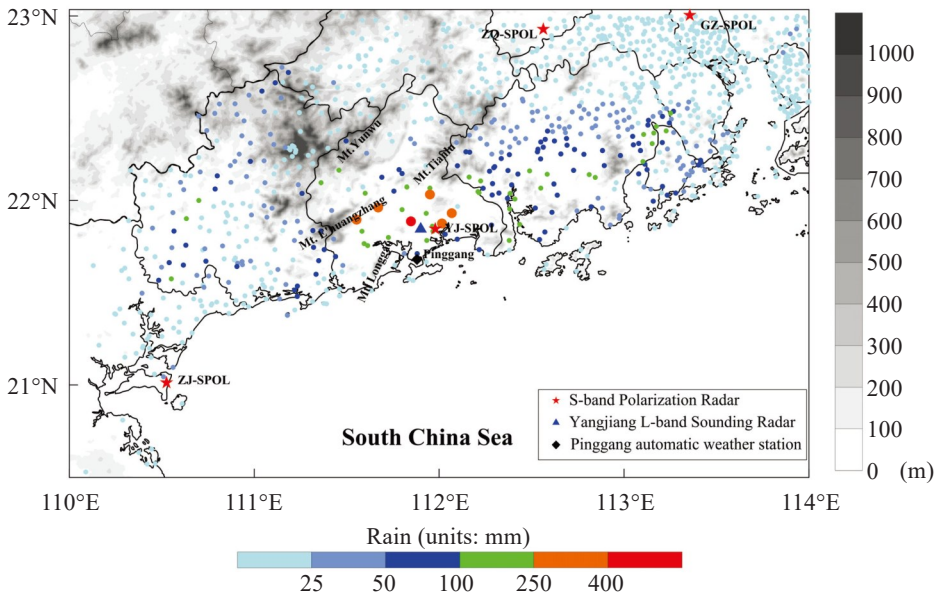

Figure 1. The 12-h (01:00-13:00 LST June 2) accumulated precipitation (units: mm, colored dots) over western Guangdong. The triangle and star marks denote the positions of the sounding and the S-band polarization radars, respectively. The terrain is shaded in grey.

of 686.97 million yuan. The heavy rainfall mainly occurred between 01:00 and 20:00 LST (=UTC+8h) on June 2, 2020. Six automatic weather stations (AWSs) in Yangjiang observed accumulated rainfall greater than 250 mm, which is consistent with the location of the heavy rainfall center on the west coast of Guangdong in the presummer rainy season (Luo et al.[33]). 17 AWSs in Jiangmen, 15 AWSs in Yangjiang, and six AWSs in other cities observed rainfall greater than 100 mm. The maximum rainfall (459.6 mm) during this event occurred in Baisha station (G2308). The maximum hourly rainfall was 98.2 mm, which was observed in Tangping station (G2319). Fig. 3b shows the temporal evolution of hourly rainfall observed at the six AWSs in Yangjiang. There were mainly two heavy rainfall periods with hourly rainfall ⩾ 20 mm. The maximum hourly rainfall reached 98.2 mm during 01:00 to 06:00 LST (the first period) and 94.7 mm during 07:00 to 13:00 LST (the second period).

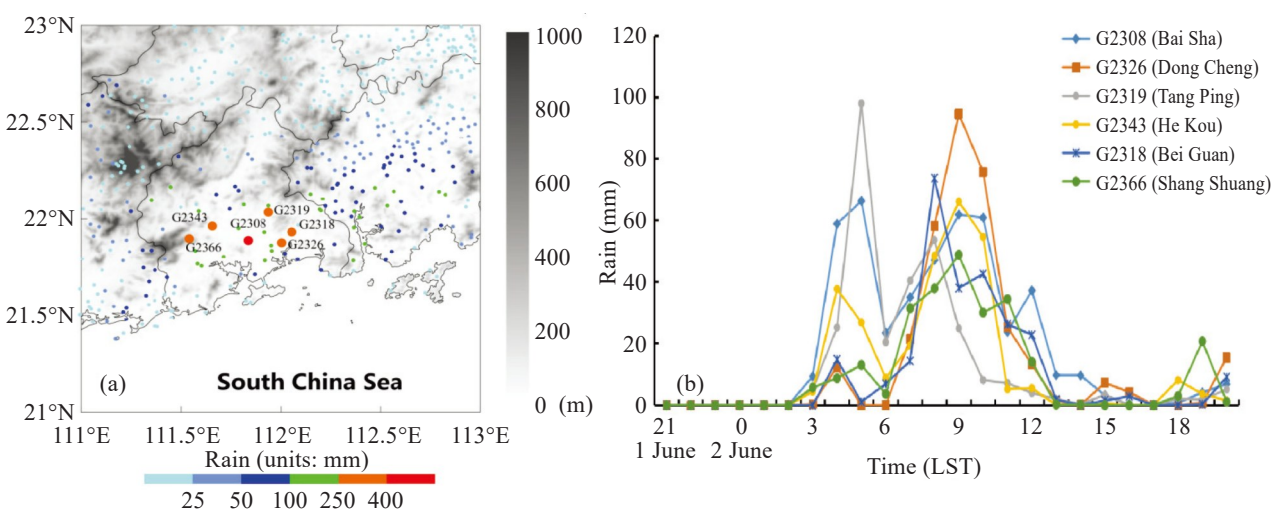

Figure 2. (a) The main heavy rainfall area. The colored dots indicate the 12-h accumulated precipitation (units: mm) as in Fig. 1. (b) Hourly precipitation (units: mm) observed by the six AWSs. The positions of the six AWSs are indicated in Fig. 2a.

3.2 *Evolution of the convective systems*

Figure 3 shows the evolution of the heavy-rain-producing convective systems. It can be found that the convective systems producing heavy rainfall in this event have gone through a change in organizational mode. In the early stage (01:06−03:30 LST), a relatively long convective band (referred to as CB1) dominated Yangjiang. In the later stage, the convective systems gradually evolved into an MRB organizational mode. After 13:00 LST, the convection weakened, became less organized, and moved away from Yangjiang, accompanied by the weakened rain.

At the beginning of this event (Fig. 3a), the convective storms were triggered near Mt. Longgao, south of Mt. Ehuangzhang and north of Hailing Island. They moved northeastwards (almost parallel to the orientation of Mt. Ehuangzhang and Longgao), and merged later. Hindered by the mountains, the convection stayed in the south of Mt. Ehuangzhang and Mt. Tianlu, presenting a nonlinear mode. At about 03:30 LST (Fig. 3b), the convective storms gradually organized into a southwest-northeast-oriented convective band (CB1), staying in the south of Mt. Ehuangzhang and Mt. Tianlu. Subsequently, convection was continuously triggered in the south of Mt. Ehuangzhang and the north of Mt. Longgao, and moved northeast to connect with the convective band. From 04:00 LST (Fig. 3c), three short convective bands were formed on the west side of CB1. These three short bands were nearly parallel to each other and they were more meridional than the long convective band. The back-building process was found at the southern end of the short convective bands, near Mt. Longgao and Mt. Ehuangzhang, which was conducive to the development of the convective systems. During the establishment of MRB mode (Fig. 3d-3e), several stations shown in Fig. 2b were in the weak echo area between the short convective bands, resulting in relatively weak precipitation at that time. At 06:06 LST (Fig. 3f), the convective storm triggered near Hailing Island and Pinggang moved northeastwards, and a new short convective band was formed. Several short convective bands present a "rainband-training" form. They moved slowly and passed some same places successively, facilitating the continuous rainfall in those areas (similar to the cases in Luo et al.[33] and Wang et al.[21]), thus resulting in the generation of heavy rainfall (Fig. 3g-3i). Later, the convective systems began to move eastward, and the new convection near Mt. Ehuangzhang, Mt. Longgao, and the north of Hailing Island gradually decreased. The convective systems and the precipitation in Yangjiang weakened (Fig. 3k-3l).

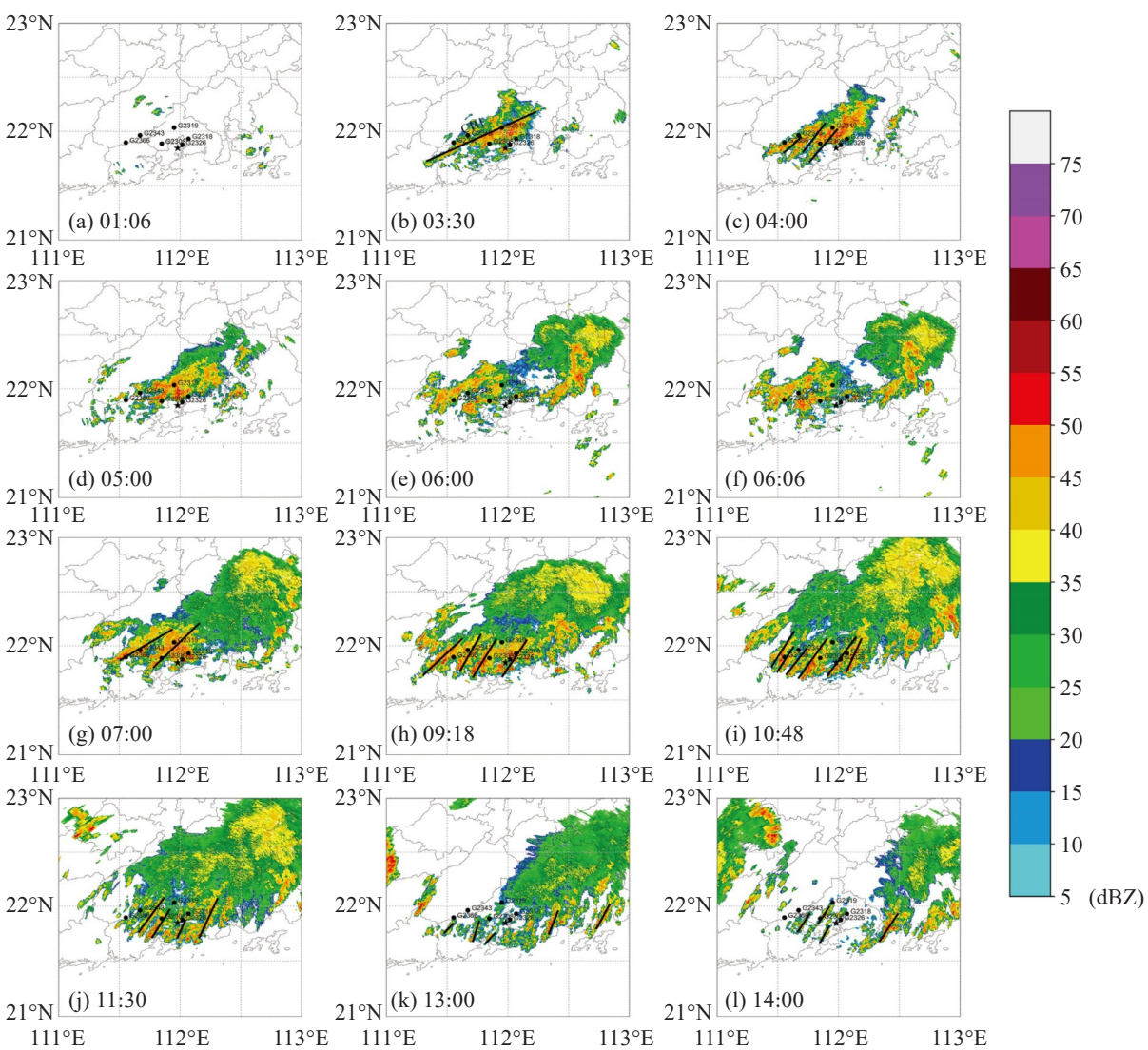

Figure 3. Radar reflectivity at 1.5 ° elevation on June 2, 2020. The Yangjiang radar is marked with a black star. The six AWSs shown in Fig. 2b are marked with black dots. (a) 01:06 LST; (b) 03:30 LST; (c) 04:00 LST; (d) 05:00 LST; (e) 06:00 LST; (f) 06:06 LST; (g) 07:00 LST; (h) 09:18 LST; (i) 10:48 LST; (j) 11:30 LST; (k) 13:00 LST; (l) 14:00 LST.

4 SYNOPTIC SITUATION AND MESOSCALE CHARACTERISTICS

4.1 *Synoptic situation*

From 00:00 to 20:00 LST June 2, the western coast of Guangdong was in the divergence region associated with anticyclonic circulation at the upper level (not shown). It was influenced by westerly-southwesterly winds in the north of the subtropical high at the middle level. In the lower troposphere, the southwesterly-southerly winds dominated the western Guangdong and the adjacent ocean (Fig. 4). The high equivalent potential temperature area gradually expanded eastwards (Fig. 4a, 4c, 4d and 4e). At 925 hPa, the wind speed increased to 12 m s^{-1}. Low-level wind convergence as well as the convergence of water vapor flux could be seen along the coast (Fig. 4b). Subsequently, the convergence zone of water vapor flux extended further east, covering the Pearl River Estuary (Fig. 4d and 4f). The continuous water vapor transport and low-level coastal convergence provided favorable conditions for the development of heavy rainfall. Convection was triggered along the east coast of Yangjiang (north of Hailing Island), and became more active later (Fig. 3e) with the enhanced convergence of water vapor flux. The cross-section along 111.75 °E (Fig. 5) shows that low-level convergence was coupled with high-level divergence in the coastal area, and there was a large vorticity area on the north side of the convergence center, which was advantageous to ascending motion. In short, the synoptic conditions were favorable for the development of heavy rainfall, although there was no distinct synoptic lifting.

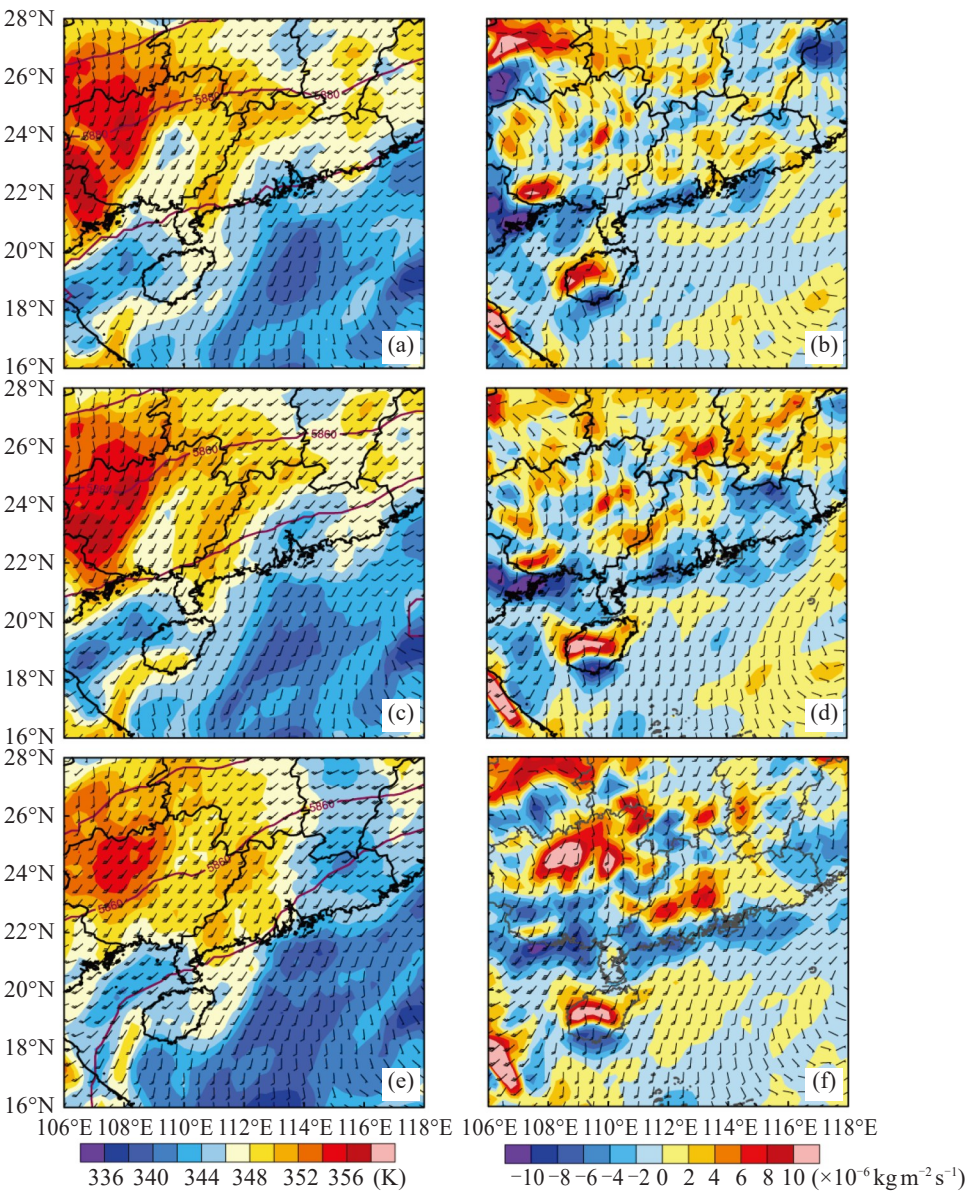

Figure 4. (a), (c) and (e): Geopotential height at 500 hPa (solid contours), winds and equivalent potential temperature (shaded) at 850 hPa; (b), (d) and (f): Integral of water vapor flux divergence below 700 hPa (shaded), and winds at 925 hPa. The first row: 00:00 LST June 2; the second row: 02:00 LST June 2; the third row: 06:00 LST June 2.

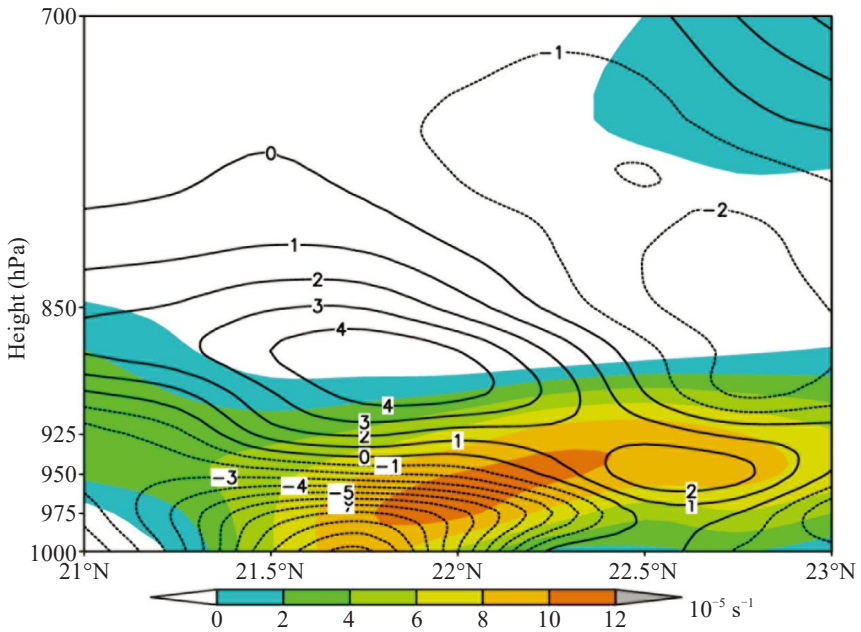

Figure 5. Cross-section of divergence (units: 10^{-5} s^{-1}; black contours, dashed for negative values, and solid for positive values) and vorticity (units: 10^{-5} s^{-1}; shaded) along 111.75 °E at 00:00 LST June 2.

Figure 6 shows the sounding in Yangjiang. At 20:00 LST June 1 (Fig. 6a), before the occurrence of this event, southerly-southwesterly winds were in the lower levels, and the winds gradually turned to be southwesterly-westerly up to 500 hPa. It was wet below 850 hPa with a dry layer at 250 − 500 hPa. The convective available potential energy (CAPE) was high (3107.8 J kg^{-1}), the convective inhibition (CIN) is small (4.6 J kg^{-1}), and the level of free convection is low (935.2 hPa), which indicates that once the uplift conditions are met, deep moist convection will be easily triggered. At 02:00 LST June 2 (Fig. 6b), the wind speed below 600 hPa increased compared with that at 20: 00 LST June 1, and the winds at 925 hPa and 700 hPa reached 16 m s^{-1}. The winds at the low levels changed to be more southerly. Almost the whole layer turned wetter. The environmental conditions were still conducive to the development of convection.

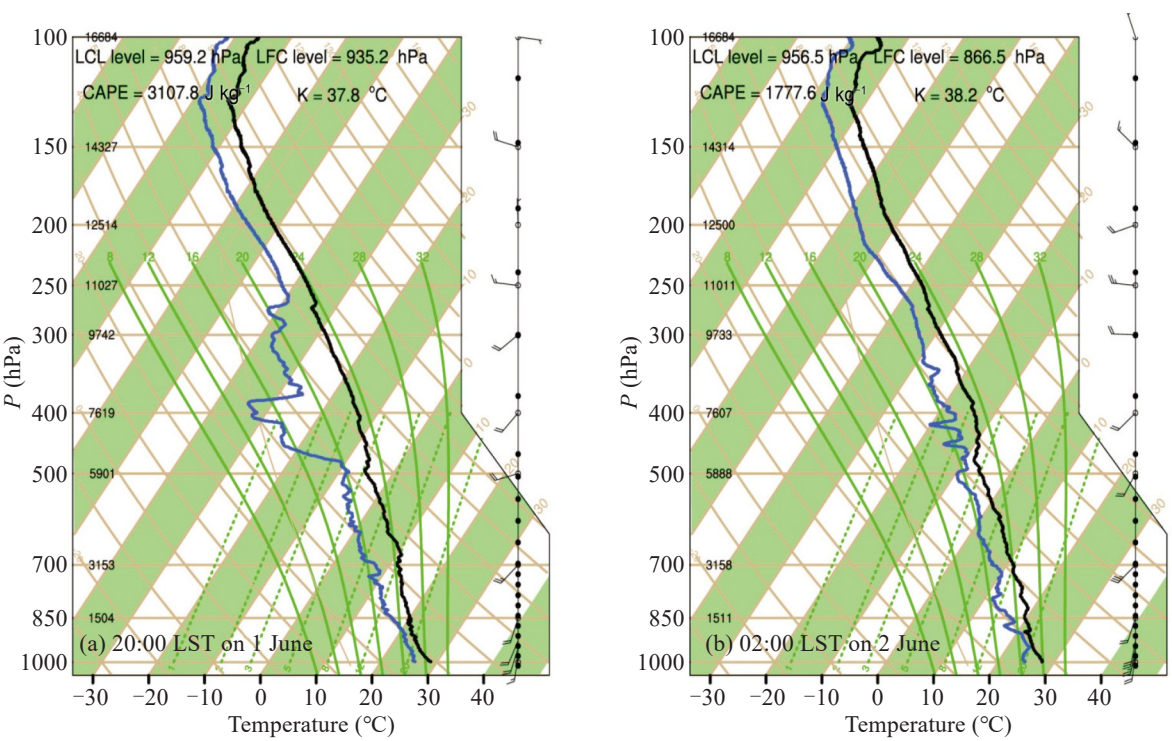

Figure 6. Sounding at the Yangjiang station at (a) 20:00 LST June 1, and (b) 02:00 LST June 2.

In order to understand the evolution of the organizational mode of the convective systems, the vector-based method proposed in Corfidi et al.[37] and Corfidi[38] was applied using the reanalysis data. Three motion vectors, i. e., the cell motion vector (C), the system motion vector (S), and the propagation vector (P), are defined with this method. C can be estimated by the mean flow in the cloud layer. P is assumed to be proportional and opposite to that of the low-level flow, or the negative of the cold pool-relative flow. And S can be obtained based on the relationship $P = S - C$. Results show that in the early stage, steered by the southwesterly flow (Fig. 7), the convective cell moved northeastwards after being triggered near the topography, while the convective system moved eastwards. It was easier for the convective bands or convective cells to merge with each other. With the increase of the southerly component of the steering winds, the convective cells tended to move towards north-northeast, and short convective bands gradually became more north-south-oriented. The short convective bands moved faster towards the southeast, and they did not merge as easily as in the earlier stage, forming the rainband-training mode.

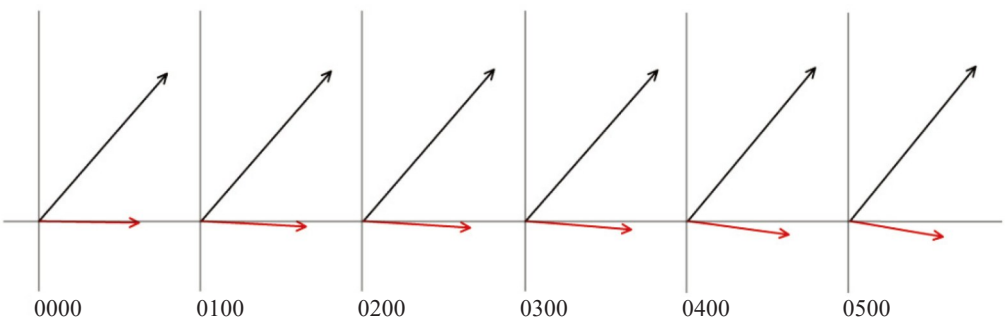

Figure 7. Hodographs from reanalysis data at 00:00, 01:00, 02:00, 03:00, 04:00, and 05:00 LST on June 2, 2020. The vectors plotted on the hodographs indicate the motion vectors of the convective cells (black vectors) and system (red vectors).

4.2 *Mesoscale circulation*

Surface observations from the AWSs show the mesoscale characteristics related to the development of convective systems (Fig. 8). At 20:00 LST June 1 (Fig. 8a), southerly winds dominated over Yangjiang. The temperature was 24−27 ℃ in the northern mountainous area, significantly lower than that in the south (27 − 29 ℃). Due to nighttime cooling, the temperature over the northern part of Yangjiang continued to decrease, and northerly land winds / mountains winds began to develop (Fig. 8b-8d). The southeasterly winds near Hailing Island turned to be southerly, with the wind speed increasing to 8 − 12 m s^{-1}. At 03:00 − 04:00 LST June 2 (Fig. 8e and 8f), under the influence of the convectively-generated cold pool, the temperature near the central part of Yangjiang dropped by 2 − 3 ℃, and winds gradually turned to be northerly-northeasterly. At the same time, the winds near the coastline continued to increase to 14−16 m s^{-1} and the temperature remained at about 28 ℃. A mesoscale convergence line between the northerly winds and southerly warm flows was found near the middle of Yangjiang, facilitating the formation of CB1 (Fig. 3c). As the cold pools expanded southwards, the temperature dropped rapidly and the wind direction changed rapidly. At 05: 00 LST, the temperature near the south of Mt. Tianlu dropped to 23 ℃. The temperature difference between the north and south of the convergence line increased to about 5 ℃. The convergence line was sustained between the cold pool outflows and southerly flows, and gradually moved southwards as the cold pools expanded. By 10:00 LST (Fig. 8i), the convergence line moved to around 21.5 °N, close to the coast. New convection was continuously triggered near the convergence line, contributing to the back-building process at the southern end of the short convective bands. At 14:00 LST (Fig. 8j), the northerly cold flows reached the coastline, and the convection weakened.

Overall, the above analysis shows that the mesoscale convergence line made a significant contribution to the formation of the relatively long convective band in the early stage and to the back-building process in the later stage.

5 MICROPHYSICAL CHARACTERISTICS

To investigate the microphysical characteristics of convection in this event, the polarimetric observations were further analyzed. The Convective Cells (CCs) were identified following Wang et al.[39]. Specifically, if the points with radar reflectivity greater than 40 dBZ exceed one-third of the total points in the column of a grid, this grid is considered as a Convective Cell (CC).

Figure 9 shows the temporal evolution of reflectivity (Z_h), differential reflectivity (Z_{DR}), and specific differential phase shift (K_{DP}). In the early stage, as the relatively long convective band was formed, the top of the 40 dBZ reflectivity layer exceeded 7 km and the maximum reflectivity was over 45 dBZ, along with large Z_{DR} and K_{DP} values (1 dB and 0.75 ° km^{-1}, respectively). Later, during the formation of the MRB

organizational mode, the height of the convection slightly decreased with the top of the 40 dBZ reflectivity layer around 6 km, and Z_{DR} was 0.8 dB below 4 km, and K_{DP} was 0.75 ° km^{-1} around 2 km. It implies that the convection during the long convective band period was relatively stronger, had larger raindrops, and produced a higher rain rate, which may be related to the more active merging process of convection.

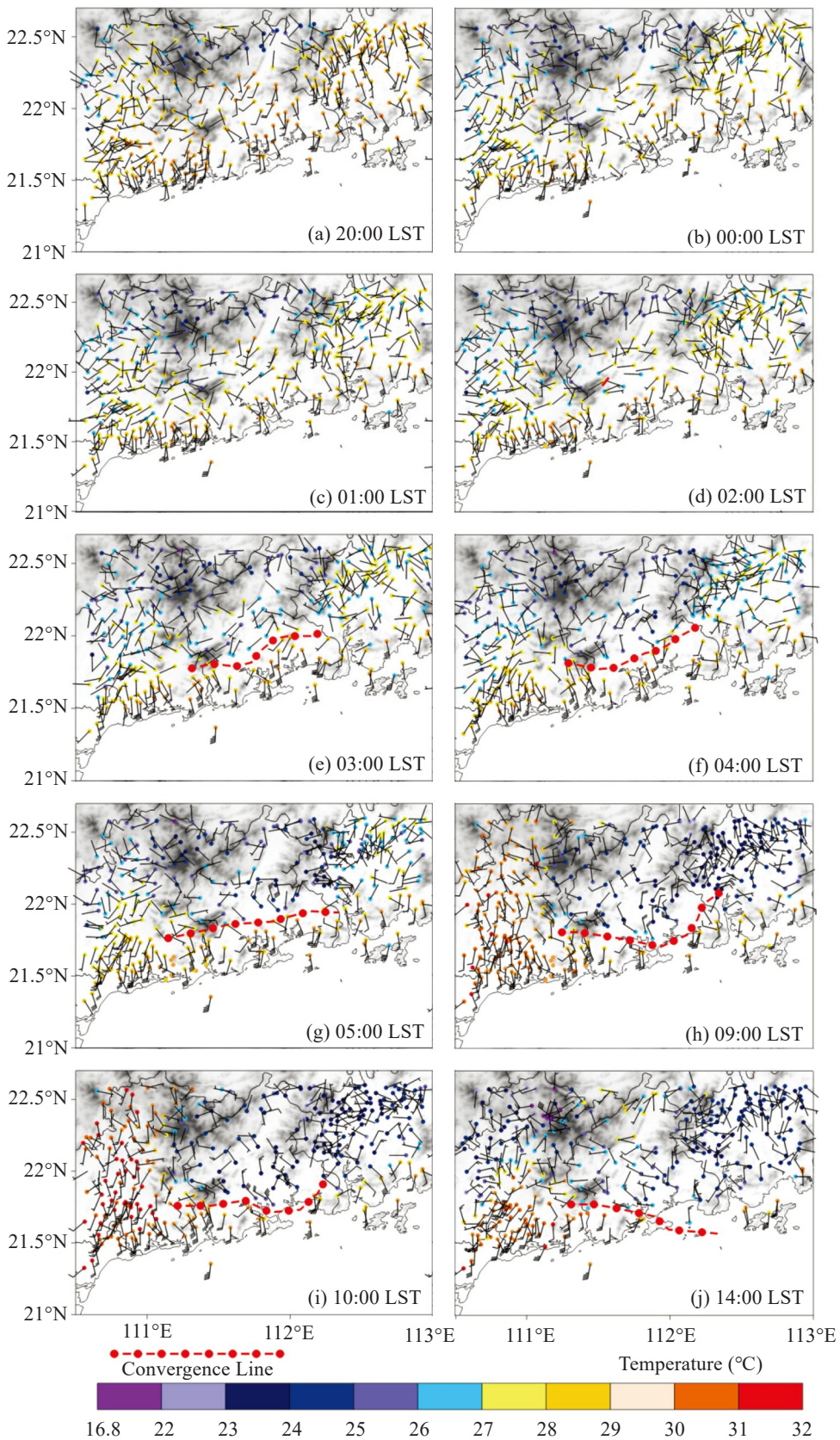

Figure 8. Temperature and winds observed by the AWSs.

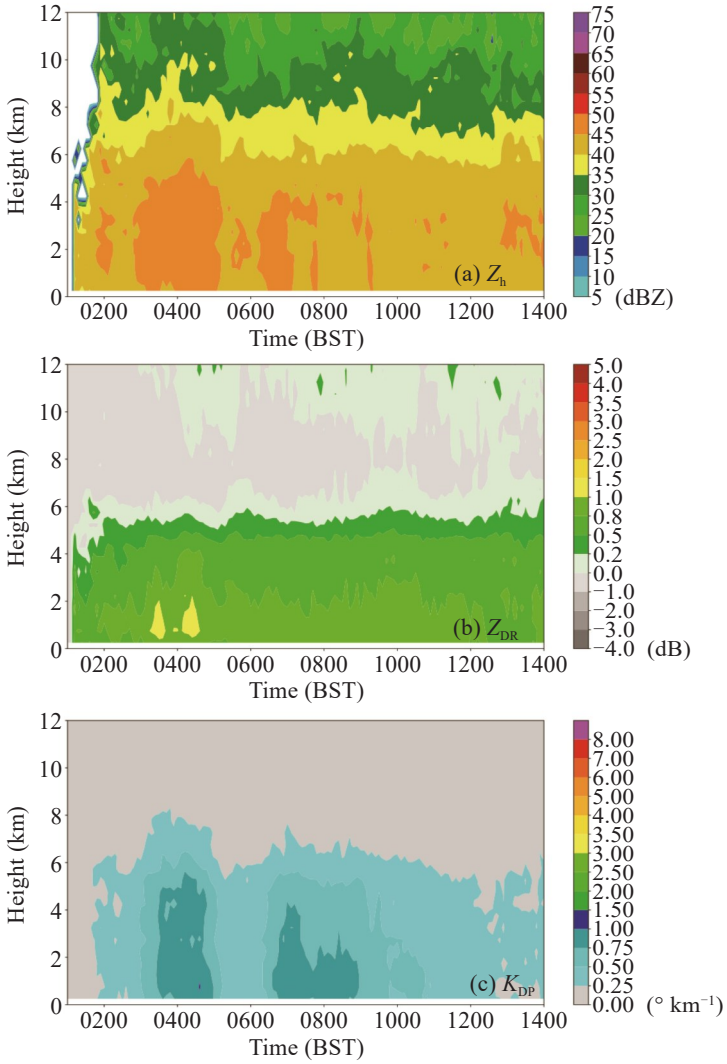

Figure 9. Time-height plots of (a) Z_h (units: dBZ), (b) Z_{DR} (units: dB), and (c) K_{DP} (units: ° km^{-1}) averaged over the CCs.

The vertical profiles of the polarimetric variables and retrieved N_w and D_m averaged over all the CCs during this event are further displayed in Fig. 10. From 6 km down to 5 km, the dramatic increase in Z_h, Z_{DR} and K_{DP} suggested an effective melting process at this level (Fig. 10a-10c). Below the freezing level, the Z_h values remained around 45 dBZ with little change while Z_{DR} and K_{DP} increased evidently with decreasing height, which indicates the active warm-rain processes (collision, and collection of cloud water by raindrops) (Kumjian and Prat[40]). From 3.5 km down to 3 km, the increase in both D_m and N_w reflected the impact of condensation and breakup processes (Fig. 10d and 10e). Below 3 km, D_m increased while N_w decreased with decreasing height, indicating that raindrops grew mainly through the collision process and that small raindrops were prone to evaporation (Dolan et al.[41]). Such features (increasing D_m and decreasing N_w towards the low level) are similar to the features during the formative stage of a squall line over east China (Wen et al.[42]) but D_m was smaller and N_w was larger in the present case. And the increasing D_m below 3 km is different from the nearly unchanged D_m below 3 km for the tropical cyclones over northeast China in 2020 (Zhang et al.[43]), suggesting that the collision process was more active in the present case.

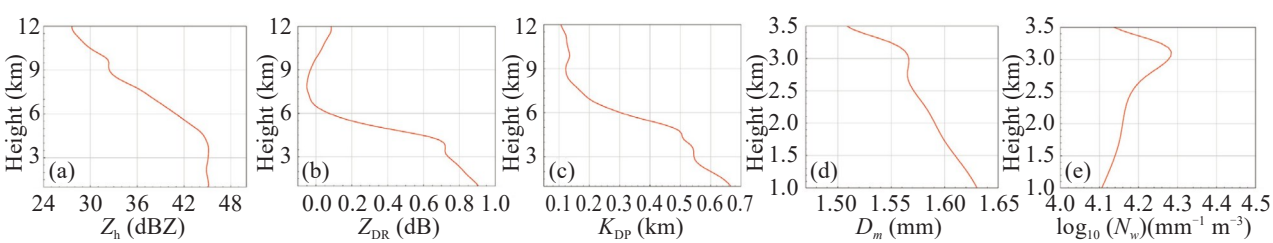

Figure 10. Average vertical profiles of (a) Z_h (units: dBZ), (b) Z_{DR} (units: dB), and (c) K_{DP} (units: ° km^{-1}), (d) D_m (units: mm), and (e) $\log_{10}(N_w)$ (units: mm^{-1} m^{-3}).

6 SUMMARY AND CONCLUSIONS

In this study, ERA5 reanalysis data, radiosonde data, AWSs, and polarimetric observations were combined to investigate a heavy rain event associated with the MRB-type convective system on June 2, 2020 along the western coast of south China.

In this event, the synoptic situation provided a favorable pre-convective environment. There were strong southwesterly flows in the lower troposphere, which transported water vapor to the rainfall area. Under the influence of the low-level southerly winds and the topography, convection was triggered continuously near the coastal mountainous area and then moved northeastwards along the southwesterly steering flows. With the nighttime cooling, the northerly winds (land winds/ mountain winds) developed near the inland mountainous area, and a mesoscale convergence line gradually formed. Under the influence of the mesoscale convergence, convection developed, and organized a relatively long southwest-northeast-oriented convection band, which was then maintained in the south of Mt. Ehuangzhang and Mt. Tianlu, resulting in the first stage of heavy precipitation. With the change in the environmental winds and the development of cold pools, three short convective bands were formed on the southwest side of the earlier long convective band, which were almost parallel to each other and close to south-north-oriented, presenting an MRB organizational mode. Supported by the cold pool outflows related to the earlier precipitation, the mesoscale convergence line maintained and gradually moved southwards. It helped trigger new convection and contributed to the back-building process at the southern end of the short convective bands near Mt. Longgao and Mt. Ehuangzhang. The heavy precipitation in this stage mainly resulted from several convective bands passing through the same place one after another. The above processes are summarized in Fig. 11. Overall, the mean flow related to the large-scale situation influenced the direction of cell motion, and the convectively-generated cold pools influenced the propagation of convection in the later stage. The initiation of new convection, the direction of cell motion, and the direction of the motion of convective bands under the influence of both large-scale situations and local circulation jointly affected the formation of MRB mode.

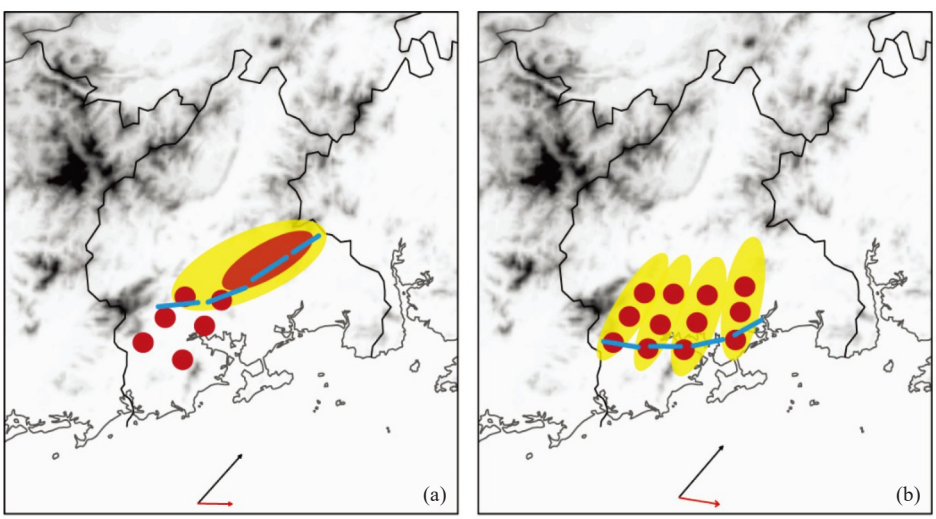

Figure 11. Conceptual diagram of the formation of the convective systems in the (a) early and (b) later stages. The red circles represent the convective cells. The yellow shadings represent the convective bands. The blue dashed lines indicate the convergence lines. The black arrows indicate the cell motion, and the red arrows indicate the motion of the convective systems.

Since the merging of convection was active, and a relatively long convective band dominated in the middle of Yangjiang city in the early stage, the convection developed to a higher level with larger raindrops. The precipitation was more in the early stage than that in the later stage. The collision process was active at low levels in this event.

In the future, it is necessary to study more cases with the MRB organizational mode, and further examine their general formation mechanisms and microphysical characteristics to provide practical information for forecasters.

REFERENCES

[1] LIN L X. Technical Guidance on Weather Forecasting in Guangdong Province [M]. Beijing: China Meteorological Press, 2006: 143-152 (in Chinese).

[2] LI J H. Ultra low-level jets and the heavy rain in early summer over south China [J]. Acta Meteorologica Sinica, 1982, 40(3): 319-326 (in Chinese), https://doi. org / 10.11676/qxxb1982.033

[3] WU M W, LUO Y L. Mesoscale observational analysis of lifting mechanism of a warm-sector convective system producing the maximal daily precipitation in China

mainland during pre-summer rainy season of 2015 [J]. Journal of Meteorological Research, 2016, 30(5): 719-736, https://doi.org/ 10.1007/s13351-016-6089-8

[4] QIAN L, DING Z Y, ZHAO X J, et al. Structure features and composite analysis of convective cells in a warm sector heavy rainfall event over southern China [J]. Journal of Tropical Meteorology, 2017, 23(3): 245-258, https://doi.org/10.16555/j.1006-8775.2017.03.002

[5] MIAO C S, YANG Y Y, WANG J H, et al. A comparative study on characteristics and thermo-dynamic development mechanisms of two types of warm-sector heavy rainfall along the south China coast [J]. Journal of Tropical Meteorology, 2018, 24(4): 494-507, https://doi. org / 10.16555/j.1006-8775.2018.04.008

[6] DU Y, CHEN G X. Heavy rainfall associated with double low-level jets over southern China. Part II: Convection initiation [J]. Monthly Weather Review, 2019, 147(2): 543-565, https://doi.org/10.1175/MWR-D-18-0102.1

[7] HUANG Y J, LIU Y B, LIU Y W, et al. Mechanisms for a record breaking rainfall in the coastal metropolitan city of Guangzhou, China [J]. Journal of Geophysical Research: Atmospheres, 2019, 124(3): 1370-1391, https://doi. org / 10.1029/2018JD030229

[8] HUANG Y J, LIU Y B, LIU Y W, et al. Budget analyses of a record-breaking rainfall event in the coastal metropolitan city of Guangzhou, China [J]. Journal of Geophysical Research: Atmospheres, 2019, 124(6): 9391-9406, https://doi.org/10.1029/2018JD030229

[9] LIANG Z M, FOVELL R G, LIU Y. Observational analysis of the characteristics of the synoptic situation and evolution of the organized warm-sector rainfall in the coastal region of south China in the pre-summer rainy season [J]. Atmosphere, 2019, 10(11): 722, https://doi.org/10.3390/atmos10110722

[10] WU Y L, GAO Y D, CHEN D H, et al. Synoptic characteristics related to warm-sector torrential rainfall events in south China during the annually first rainy season [J]. Journal of Tropical Meteorology, 2020, 26(3): 253-260, https://doi.org/10.46267/j.1006-8775.2020.023

[11] LIANG Z M, GAO S T. Organized warm-sector rainfall in the coastal region of south China in an anticyclone synoptic situation: Observational analysis [J]. Journal of Meteorological Research, 2021, 35(3): 460-477, https://doi.org/10.1007/s13351-021-0157-4

[12] DU Y, SHEN Y, CHEN G X. Influence of coastal marine boundary layer jets on rainfall in south China [J]. Advances in Atmospheric Sciences, 2022, 39(5): 782-801, https://doi.org/10.1007/s00376-021-1195-7

[13] WU N G, DING X, WEN Z P, et al. Contrasting frontal and warm-sector heavy rainfalls over South China during the early-summer rainy season [J]. Atmospheric Research, 2020, 235: 104693, https://doi. org / 10.1016 / j. atmosres.2019.104693

[14] WANG C L, ZHAO K, HUANG A N, et al. The crucial role of synoptic pattern in determining the spatial distribution and diurnal cycle of heavy rainfall over the south China coast [J]. Journal of Climate, 2021, 34(7): 2441-2458, https://doi.org/10.1175/JCLI-D-20-0274.1

[15] DU Y, CHEN G X, HAN B, et al. Convection initiation and growth at the coast of south China. Part II: Effects of the terrain, coastline and cold pools [J]. Monthly Weather Review, 2020, 148(9): 3871-3892, https://doi.org/10.1175/MWR-D-20-0090.1

[16] YIN J F, ZHANG D L, LUO Y L, et al. On the extreme rainfall event of 7 May 2017 over the coastal city of Guangzhou. Part I: Impacts of urbanization and orography [J]. Monthly Weather Review, 2020, 148(3): 955-979, https://doi.org/10.1175/MWR-D-19-0212.1

[17] LI H Q, HUANG Y J, HU S, et al. Roles of terrain, surface roughness, and cold pool outflows in an extreme rainfall event over the coastal region of south China [J]. Journal of Geophysical Research: Atmospheres, 2021, 126 (23): e2021JD035556, https://doi. org / 10.1029 / 2021JD035556

[18] GAO X Y, LUO Y L, LIN Y L, et al. A source of WRF simulation error for the early-summer warm-sector heavy rainfall over south China coast: Land-sea thermal contrast in the boundary layer [J]. Journal of Geophysical Research: Atmospheres, 2022, 127(4): e2021JD035179, https://doi.org/10.1029/2021JD035179

[19] ZHANG M R, RASMUSSEN K L, MENG Z Y, et al. Impacts of coastal terrain on warm-sector heavy-rain-producing MCSs in southern China [J]. Monthly Weather Review, 2022, 150(3): 603-624, https://doi.org/10.1175/MWR-D-21-0190.1

[20] HE L F, CHEN T, KONG Q. A review of studies on prefrontal torrential rain in south China [J]. Journal of Applied Meteorological Science, 2016, 27(5): 559-569, https://doi.org/10.11898/1001-7313.20160505

[21] WANG H, LUO Y L, JOU B J D. Initiation, maintenance, and properties of convection in an extreme rainfall event during SCMREX: Observational analysis [J]. Journal of Geophysical Research: Atmospheres, 2014, 119(23): 13206-13232, https://doi.org/10.1002/2014JD022339

[22] LI S, MENG Z Y, WU N G. A preliminary study on the organizational modes of mesoscale convective systems associated with warm-sector heavy rainfall in south China [J]. Journal of Geophysical Research: Atmospheres, 2021, 126(16): e2021JD034587, https://doi. org / 10.1029 / 2021JD034587

[23] PARKER M D, JOHNSON R H. Organizational modes of midlatitude mesoscale convective systems [J]. Monthly Weather Review, 2000, 128(10): 3413-3436, https://doi.org/10.1175/1520-0493(2001)129<3413:OMOMMC>2.0.CO;2

[24] SCHUMACHER R S, JOHNSON R H. Organization and environmental properties of extreme-rain-producing mesoscale convective systems [J]. Monthly Weather Review, 2005, 133(4): 961-976, https://doi.org/10.1175/MWR2899.1

[25] GALLUS Jr W A, SNOOK N A, JOHNSON E V. Spring and summer severe weather reports over the Midwest as a function of convective mode: A preliminary study [J]. Weather and Forecasting, 2008, 23(1): 101-113, https://doi.org/10.1175/2007WAF2006120.1

[26] ZHENG L L, SUN J H, ZHANG X L, et al. Organizational modes of mesoscale convective systems over central east China [J]. Weather and Forecasting, 2013, 28(5): 1081-1098, https://doi.org/10.1175/WAF-D-12-00088.1

[27] LIU X, LUO Y L, GUAN Z Y, et al. An extreme rainfall event in coastal south China during SCMREX-2014: Formation and roles of rainband and echo trainings [J]. Journal of Geophysical Research: Atmospheres, 2018,

123(17): 9256-9278, https://doi. org / 10.1029 / 2018JD028418

[28] ZHAO K, HUANG H, WANG M J, et al. Recent progress in dual-polarization radar research and applications in China [J]. Advances in Atmospheric Sciences, 2019, 36 (9): 961-974, https://doi.org/10.1007/s00376-019-9057-2

[29] LIU X T, RUAN Z, HU S, et al. The Longmen Cloud Physics Field Experiment Base, China Meteorological Administration [J]. Journal of Tropical Meteorology, 2023, 29(1): 1-15, https://doi. org / 10.46267 / j. 1006-8775.2023.001

[30] LI M X, LUO Y L, ZHANG D L, et al. Analysis of a record-breaking rainfall event associated with a monsoon coastal megacity of south China using multisource data [J]. IEEE Transactions on Geoscience and Remote Sensing, 2021, 59(8): 6404-6414, https://doi.org/10.1109/TGRS.2020.3029831

[31] HAN B, DU Y, WU C, et al. Microphysical characteristics of the coexisting frontal and warm-sector heavy rainfall in south China [J]. Journal of Geophysical Research: Atmospheres, 2021, 126(21): e2021JD035446, https://doi.org/10.1029/2021JD035446

[32] WANG H, YIN J F, WU N G, et al. Microphysical structures of an extreme rainfall event over the coastal metropolitan city of Guangzhou, China: Observation analysis with polarimetric radar [J]. Asia-Pacific Journal of Atmospheric Sciences, 2023, 59: 3-16, https://doi.org/10.1007/s13143-022-00289-y

[33] LUO Y L, ZHANG R H, WAN Q L, et al. The Southern China Monsoon Rainfall Experiment (SCMREX) [J]. Bulletin of the American Meteorological Society, 2017, 98 (5): 999-1013, https://doi. org / 10.1175 / BAMS-D-15-00235.1

[34] ZHANG J, HOWARD K, GOURLEY J J. Constructing three-dimensional multiple-radar reflectivity mosaics: Examples of convective storms and stratiform rain echoes [J]. Journal of Atmospheric and Oceanic Technology, 2005, 22(1): 30-42, https://doi.org/10.1175/jtech-1689.1

[35] ZHANG G F, VIVEKANANDAN J, BRANDES E. A method for estimating rain rate and drop size distribution from polarimetric radar measurements [J]. IEEE Transactions on Geoscience and Remote Sensing, 2001, 39(4): 830-841, https://doi.org/10.1109/36.917906

[36] LIU X T, WAN Q L, WANG H, et al. Raindrop size distribution parameters retrieved from Guangzhou S-band polarimetric radar observations [J]. Journal of Meteorological Research, 2018, 32(4): 571-583, https://doi.org/10.1007/s13351-018-7152-4

[37] CORFIDI S F, MERITT J H, FRITSCH J M. Predicting the movement of mesoscale convective complexes [J]. Weather and Forecasting, 1996, 11(1): 41-46, https://doi.org / 10.1175 / 1520-0434(1996)011<0041: PTMOMC>2.0.CO;2

[38] CORFIDI S F. Cold pools and MCS propagation: Forecasting the motion of downwind-developing MCSs [J]. Weather and Forecasting, 2003, 18(6): 997-1017, https://doi. org / 10.1175 / 1520-0434(2003)018<0997: CPAMPF>2.0.CO;2

[39] WANG H, KONG F Y, WU N G, et al. An investigation into microphysical structure of a squall line in South China observed with a polarimetric radar and a disdrometer [J]. Atmospheric Research, 2019, 226(15): 171-180, https://doi.org/10.1016/j.atmosres.2019.04.009

[40] KUMJIAN M R, PRAT O P. The impact of raindrop collisional processes on the polarimetric radar variables [J]. Journal of the Atmospheric Sciences, 2014, 71(8): 3052-3067, https://doi.org/10.1175/JAS-D-13-0357.1

[41] DOLAN B, RUTLEDGE S A, LIM S, et al. A robust C-band hydrometeor identification algorithm and application to a long-term polarimetric radar dataset [J]. Journal of Applied Meteorology and Climatology, 2013, 52(9): 2162-2186, https://doi. org / 10.1175 / JAMC-D-12-0275.1

[42] WEN J, ZHAO K, HUANG H, et al. Evolution of microphysical structure of a subtropical squall line observed by a polarimetric radar and a disdrometer during OPACC in Eastern China [J]. Journal of Geophysical Research: Atmospheres, 2017, 122(15): 8033-8050, https://doi.org/10.1002/2016JD026346

[43] ZHANG A Q, CHEN Y L PAN X, et al. Precipitation microphysics of tropical cyclones over Northeast China in 2020 [J]. Remote Sensing, 2022, 14(9): 2188, https://doi.org/10.3390/rs14092188

Citation: ZHANG Hong-hao, GUO Ze-yong, LI Hui-qi, et al. Study on the Formation Mechanism and Microphysical Characteristics of Warm-Sector Convective System with Multiple-Rain-Bands Organizational Mode [J]. Journal of Tropical Meteorology, 2023, 29(2): 252-263, https://doi.org/10.46267/j.1006-8775.2023.018